Structural Basis for the Enantioselectivity of Esterase Est-Y29 toward (S)-Ketoprofen

Journal:	*ACS Catalysis*
Manuscript ID	cs-2018-02797v.R1
Manuscript Type:	Article
Date Submitted by the Author:	03-Dec-2018
Complete List of Authors:	Ngo, Tri; Sungkyunkwan University School of Medicine Oh, Changsuk; Sungkyunkwan University School of Medicine, Dept. of Molecular Cell Biology Mizar, Pushpak ; University of Southampton, Chemistry Baek, Minkyung ; Seoul National University Park, Kwang-su; Konkuk University, Dept. of Bioscience & Biotechnology Nguyen, Lan; Sungkyunkwan University School of Medicine, Molecular Cell Biology Byeon, Huimyoung; Sungkyunkwan University - Suwon Campus, Energy Science Yoon, Sangyoung; Ajou University Ryu, Yeonwoo; Ajou University Ryu, Bum Han; Sungkyunkwan University School of Medicine, Molecular Cell Biology Kim, T. Doohun ; Sookmyung Women's University Yang, Jung Woon; Sungkyunkwan University - Suwon Campus, Energy Science Seok, Chaok; Seoul National University, Department of Chemistry Lee, Seung Seo; University of Southampton, Chemistry Kim, Kyeong; Sungkyunkwan University School of Medicine, Molecular Cell Biology

Structural Basis for the Enantioselectivity of Esterase Est-Y29 toward (*S*)-Ketoprofen

Tri Duc Ngo[1$], Changsuk Oh[1$], Pushpak Mizar[2], Minkyung Baek[3], Kwang-su Park[1], Lan Nguyen[1], Huimyoung Byeon[4], Sangyoung Yoon[5], Yeonwoo Ryu[5], Bum Han Ryu[1], T. Doohun Kim[6], Jung Woon Yang[4], Chaok Seok[3], Seung Seo Lee[2], Kyeong Kyu Kim[1*]

[1]Department of Molecular Cell Biology, Sungkyunkwan University School of Medicine, Suwon, 16419, Republic of Korea; [2]Chemistry, Highfield Campus, University of Southampton, Southampton, SO17 1BJ, UK. [3]Department of Chemistry, College of Natural Sciences, Seoul National University, Seoul, 08826, Republic of Korea; [4]Department of Energy, Sungkyunkwan University, Suwon, 16419, Republic of Korea; [5]Department of Applied Chemistry & Biological Engineering, Ajou University, Suwon, 16499, Republic of Korea; [6]Department of Chemistry, College of Natural Sciences, Sookmyung Women's University, Seoul, 04310, Republic of Korea

Abstract

The thermostable esterase Est-Y29, belonging to the family VIII lipolytic esterase isolated from metagenomes extracted from the topsoil in Republic of Korea, was identified as a promising catalyst for the production of (*S*)-ketoprofen, an important nonsteroidal anti-inflammatory drug (NSAID). For industrial applications, the enantioselectivity of the enzyme towards the *S*-enantiomer of the racemic ketoprofen ester substrate needs to be improved. To understand the structural basis of Est-Y29 enantioselectivity, which is necessary for the rational design of an enzyme with enhanced enantioselectivity, we solved the crystal structures of Est-Y29 bound to *(S)*-ketoprofen at 1.69 Å resolution. Structural analyses revealed that the *S*-enantiomer can be stabilized by a π-interaction between the methyl substituent at the chiral carbon of the ligand and the aromatic pocket formed by Tyr123, Phe125, and Tyr170. This finding is further supported by the highly improved enantioselectivity of the mutant Est-Y29 (F125W) toward (*S*)-ketoprofen due to the enhanced π-interaction. Our results provide the molecular basis of the enantioselectivity of Est-Y29 against (*S*)-ketoprofen and further offer the opportunity for the rational design of enzyme enantioselectivity as well as potential applications of the mutant Est-Y29 to industrial biocatalysts.

Key words: crystal structure, esterase, Est-Y29, rational design, enantioselectivity, (*S*)-ketoprofen

1. Introduction

Biocatalysts have been under development for several decades to replace chemical-based synthesis because they have advantages in economic feasibility and environmental friendliness [1]. In addition, their higher specificity in regio- and stereo-isomers is useful for reducing synthesizing steps, which is a key consideration for industrial applications of biocatalysts. Therefore, high stereoselectivity is one of the most important functional features for using enzymes as biocatalysts.

Many biochemical features of enzymes such as stability, activity, and selectivity must be considered for their various industrial applications from pharmaceuticals and green chemistry to biofuels [2-3]. To improve enzyme properties for industrial applications, two strategies have been widely used: directed evolution and rational design. Directed evolution, conducted by a combination of random mutagenesis and high-throughput screening, can be applied when structural information is not available and the assay system is well established [4-9]. Conversely, rational design relies on the availability of structural information and the knowledge of catalytic mechanisms [10-13]. Although directed evolution has emerged as a popular tool in this field, it has limitations in that a huge number of random mutants, whose numbers exponentially increase in direct relation to the number of amino acids in the enzyme, must be screened to cover all possible combinations. Therefore, when the information of structures and enzyme mechanisms is available, rational design has proven to be an effective approach. In the rational design approach to acquire the enhanced enantioselectivity, the principle of mutation is to either stabilize the faster-reacting enantiomers or to destabilize the slower-reacting ones in the transition state by mutating the residues that affect interaction between the residues and any substituents at the chiral carbon of substrates [10, 13].

Ketoprofen [2-(3-benzoylphenyl)-propionic acid], a non-selective inhibitor of cyclooxygenases (COXs), has been widely used as a non-steroidal anti-inflammatory drug

(NSAID) [14-15]. There are two stereoisomers of ketoprofen with one chiral center: (*R*)-(-)- and (*S*)-(+)-forms. In terms of inhibitory power to COXs, (*S*)-ketoprofen was shown to be 100 times stronger than (*R*)-ketoprofen [16]. Subsequent studies also revealed that the *S*-enantiomer had higher suppressive effects of PGE_2 production in macrophages and to edema, whereas the *R*-enantiomer only showed effects as a pain killer [17-18]. (*R*)-ketoprofen has also been used as an additive in a toothpaste for the purpose of reducing periodontal disease [19]. Due to differences in physiological functions of ketoprofen isomers, the Food and Drug Administration (FDA) requested to separate each enantiomer for specific usage [20-21]. Ong *et al*. summarized several approaches for the effective production of the (*S*)-enantiomer of ketoprofen, including diastereomer crystallization, kinetic resolution, asymmetric synthesis, chromatography separation, and preferential crystallization [22]. Among them, kinetic resolution by enantio-specific esterification or hydrolysis has been most widely used because it has no unexpected side product and is an environment-friendly process with efficient processing steps.

Est-Y29, a family VIII lipolytic esterase isolated from metagenomes, isolated from the topsoil in the area of Chungcheong-bukdo, Republic of Korea (Microbial Genomics and Application Center, Republic of Korea), showed moderated enantioselectivity against (*S*)-ketoprofen ethyl ester (Scheme 1) [23]. This enzyme is a promising catalyst for producing the medicinally active enantiomer of ketoprofen due to its high stability in organic solvents, acidic and basic conditions, and high temperature conditions [23]. However, since the enantioselectivity of Est-Y29 was only marginal (*E* value = 4.48), its enantioselectivity must be improved to use Est-Y29 as a biocatalyst for producing (*S*)-ketoprofen. Previously we solved the crystal structures of Est-Y29 in apo (PDB code: 4P6B) and inhibitor-bound (PDB code: 4P87) forms, which reveal that Est-Y29 belongs to the α/β hydrolase fold with S58-K61-Y170 catalytic triad [24-25]. For the purpose of applying a rational design approach to improve the enantioselectivity of Est-Y29, we solved the crystal structures of Est-Y29 in complexes with (*S*)-ketoprofen. In

addition to the structural interpretation of the complex structure, based on the docking studies of (*R*)- and (*S*)-ketoprofens ethyl ester and structural analyses of Est-Y29 mutants in a complex with (*S*)-ketoprofen ethyl ester, we found the structural bases for the enantioselectivity of Est-Y29. Furthermore, by this approach, we designed a mutant that has 5-fold higher enantioselectivity than the wild-type Est-Y29. Therefore, this study not only provides the molecular basis for the enantioselectivity of the ester hydrolysis enzyme but also produces a potential biocatalyst with an industrial application for the synthesis of a medicinally active enantiomer of ketoprofen.

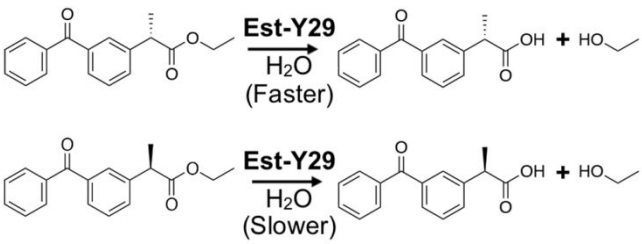

Scheme 1. Enantioselective Hydrolysis of Racemic (*R*,*S*)-Ketoprofen Ethyl Ester by Esterase Est-Y29

2. Materials and Methods

2.1 Preparation of Racemic and (*S*)-Ketoprofen Ethyl Ester

Substrates for Est-Y29 and its mutants were prepared from commercially available (*S*)-ketoprofen (Sigma-Aldrich, MO, USA), (*R*)-ketoprofen (Toronto Research Chemicals, ON, Canada), and racemic ketoprofen (Tokyo Chemical Industry, Japan). As previous description for esterification [26], 0.2 mM of racemic ketoprofen dissolved in 2 mL of ethanol was incubated at 333 K for 5 h with a 10 μL of concentrated sulfuric acid as a catalyst. After removal of residual ethanol by heating *in vacuo*, the mixture was poured into saturated $NaHCO_3$, and the aqueous layer was extracted with ethyl acetate. The combined organic phases were washed with brine, dried over Na_2SO_4, filtrated, and concentrated under reduced pressure. The residue was purified by flash chromatography on silica gel using 1:3 mixture of ethyl acetate and hexanes to give racemic ketoprofen ethyl ester as light yellowish liquid. The structure of racemic ketoprofen ethyl ester was confirmed by ^{1}H and ^{13}C NMR spectroscopy (Figure S1). (*S*)-ketoprofen ethyl ester and (*R*)-ketoprofen ethyl ester were also prepared in the same procedure.

2.2 Protein Purification and Crystallization

Protein expression and purification were performed as described elsewhere with slight modifications[24]. Briefly, the pQE30-Est-Y29 construct was transformed into *Escherichia coli* XL1-Blue cells (Agilent, CA, USA) inoculated in 500 mL of LB medium containing 100 $\mu g \cdot mL^{-1}$ ampicillin. Protein induction was performed at 310K for 4 h using 1 mM isopropyl-β-D-1-thiogalactoside (IPTG) as final concentration. Cells were harvested through centrifugation at 6,000 g for 15 min, suspended in buffer A (50 mM Tris-HCl, 300 mM NaCl with 50 mM imidazole a pH8.0), and disrupted by sonication. After centrifugation at 69,000 g

for 30 min, the supernatant was applied to a Ni-NTA column (GE Healthcare, IL, USA) equilibrated with the buffer A, followed by an extensive washing step using buffer A to remove non-specifically bound proteins. Subsequently, the bound protein was eluted using 150-450 mM of imidazole-gradient buffer A, and from the collected protein, homogenous Est-Y29 was obtained using HiLoad 16/600 Superdex 200 column (GE Healthcare, IL, USA) with 10 mM phosphate buffer pH 8.0. The finally purified Est-Y29 was concentrated to 10 $mg \cdot mL^{-1}$ with buffer change using an Amicon Ultra-15 centrifugal filter, 10 kDa MWCO (Merk Millipore, Germany), and stored at 193 K until the next use. Purification of Est-Y29 mutants (F125W, R225A and A348V) was performed in the same way as that of native protein.

Crystallization was performed using the microbatch (Thermo Fisher Scientific, Denmark) crystallization method under a thin layer of Al's oil, using commercially available screening kits from Hampton Research (Hampton Research, CA, USA) at 295 K. Est-Y29 was mixed with (*S*)-ketoprofen ethyl ester to a final concentration of 8 $mg \cdot mL^{-1}$ for protein and 1 mM for (*S*)-ketoprofen ethyl ester and incubated 5 min before crystal setting. Diffraction-quality crystals of Est-Y29 F125W and a complex of Est-Y29 with (*S*)-ketoprofen (Est-Y29-SKP) were obtained from the reservoir containing 1 M sodium citrate and 100 mM sodium acetate pH 4.6 after one day incubation at 287K. We used the same approach to crystallize complexes of Est-Y29 A348V with (*S)*-ketoprofen ethyl ester (Est-Y29 A348V-SKE) with Est-Y29-SKP except we increased the incubation time to 30 min.

2.3 X-ray Data Collection

Crystals of the complex of Est-Y29-SKP, Est-Y29 F125W and Est-Y29 A348V-SKE were transferred to a cryosolution containing 1 M sodium citrate, 100 mM sodium acetate pH 4.6, 25% glycerol, and 1 mM (*S)*-ketoprofen ethyl ester. X-ray diffraction data were collected at 100 K using an ADSC Quantum 210 detector on beamline NW12 at Photon Factory (PF) in

Japan and an ADSC Quantum 315 CCD on beamline PAL 7A at the Pohang Accelerator Laboratory (PAL) in Korea. The data were indexed, integrated, and scaled using HKL-2000 [27]. Data collection and processing statistics for Est-Y29-SKP, Est-Y29 F125W, and Est-Y29 A348V-SKE are summarized in Table 1.

2.4 Structure Determination and Refinement

The structure of apo-Est-Y29 (PDB code: 4P6B) was used as a template for molecular replacement to solve the structure of Est-Y29-SKP, Est-Y29 F125W and Est-Y29 A348V-SKE using MOLREP [28]. The model was refined using REFMAC [29-30] and PHENIX [31]. The quality of the final model was evaluated with the program PROCHECK [32]. Refinement statistics are given in Table 1. The structure models were described using PyMOL, and interactions between protein and ligand were visualized using *BIOVIA Discovery Studio* (Accelrys, CA, USA). The final models Est-Y29-SKP (PDB code: 5ZWR), Est-Y29 F125W (PDB code: 5ZWV) and Est-Y29 A348V-SKE (PDB code: 5ZWQ) were deposited in PDB.

Table 1. Data Collection and Refinement of the Complex Structures of Est-Y29-SKP and Mutants, Est-Y29 F125W and Est-Y29 A348V-SKE[a].

	Est-Y29-SKP (5ZWR)	Est-Y29 F125W (5ZWV)	Est-Y29 A348V-SKE (5ZWQ)
Data Collection			
Space Group	*I*4	*I*4	*I*4
Cell Dimensions			
a, *b*, *c* (Å)	122.3, 122.3, 155.8	121.8, 121.8, 155.4	122.3, 122.3, 155.2
α, β, γ (°)	90.0, 90.0, 90.0	90.0, 90.0, 90.0	90.0, 90.0, 90.0
Molecules/AU	2	2	2

Wavelength	1.0000	1.0000	1.0000
Resolution (Å)	50-1.69	50 - 2.10	50 - 1.80
R_{sym} or R_{merge}[b]	5.2 (29.2)	8.0 (31.7)	8.0 (37.8)
Mean $I/\sigma(I)$	49.9 (8.3)	34.5 (8.1)	24.7 (3.4)
Completeness (%)	99.9 (99.9)	99.9 (99.7)	99.7 (98.4)
Redundancy	7.4 (7.3)	7.5 (7.5)	3.7 (3.7)
Refinement			
Resolution (Å)	50 – 1.69	50 – 2.10	50 – 1.80
No. Reflections	127264	65885	105315
R_{work}[c] / R_{free}[d]	15.57/17.78	15.01/19.01	16.22/18.87
No. Atoms			
Protein	6122	6040	5996
Ligand/Ion	50	-	54
Water	1124	797	827
B-factors			
Protein	16.54	21.80	21.04
Ligand/Ion	26.07	-	42.59
Clash Score	3.69	2.09	2.01
R.M.S.D.[e]			
Bond Lengths (Å)	0.007	0.007	0.012
Bond Angles (°)	1.047	0.833	1.159
Ramachandran (%)			
Favored	97.6	96.77	97.01

Allowed	2.33	3.23	2.99
Outliers	0.00	0.00	0.00

[a] Values in parentheses refer to the last resolution shell.

[b] $R_{symm} = \sum_h \sum_i | I(h_i) - \langle I(h) \rangle | / \sum_h \sum_i I(h_i)$, where $I(h_i)$ is the single intensity of reflection h as determined by the ith measurement and $\langle I(h) \rangle$ is the mean intensity of reflections h.

[c] R_{work} (%) $= \sum | F_O - F_C | / \sum F_O$, where, F_O is the observed structure factor amplitude and F_C is the structure factor calculated from the model.

[d] R_{free} (%) is calculated in the same manner as R_{work} using 5% of all reflections excluded from refinement stages using high resolution data.

[e] R.M.S.D., root-mean-square deviation.

2.5 Structure Analysis

The distances between two interacting atoms or center of aromatic rings were calculated using the Discovery Studio (Accelrys, CA, USA). Hydrogen bonds, π–interactions (π-σ, π-π, and π-alkyl), salt-bridges were identified based on the type of interaction and their distances in the Discovery Studio. The default values were used. Cavity volumes of the wild-type, and mutant EST-Y29 were calculated using CASTp3.0 [33] after removing the bound ligands in the case of the wild-type enzyme. For the calculation of the cavity volume of the F125W mutant, F125 in the wild-type structure was mutated to tryptophan residue followed by energy minimization since residues 225-227 in the flexible loop occupy the active site cavity.

2.6 Docking Simulation

The crystal structure of Est-Y29-SKP was used as a docking template for the docking to the wild-type and F125W EST-Y29. The crystal structure of the A348V mutant bound to SKE was used for the docking template for the docking to the A348V mutant. All resolved water molecules were removed from the structure prior to protein preparation and subsequent docking simulations. Template structures were minimized using L-BFGS-B with GalaxyRefine[34] energy before docking was performed. The F125W mutant structure was prepared by mutating F125 of wild type enzyme to tryptophan residue followed by local minimization using L-BFGS-B.

AutoDock Tool [35] was used to create a .pdbqt file, which is a modified PDB file containing 1) the coordinates of protein and substrates, (*S*)-ketoprofen ethyl ester and (*R*) -ketoprofen ethyl ester, and 2) additional information such as partial charges, atom type, and topology. Substrate docking to the Est-Y29 was performed using *AutoDock Vina* [36] with W125, R225, and L227 defined as flexible side chains. Subsequently, the docking space was visually defined in *AutoDock Tool*. The grid box around the catalytic triads with a dimension of 20 Å x 32 Å x 20 Å was used to cover the entire substrate-binding site and to accommodate ligands. Defaults parameters were used during the ligand docking except exhaustiveness, which was adjusted to 1000. Calculations for ligand docking were done using the Lamarckian Genetic Algorithm (LGA) method [37]. Among the top 10 candidates, the final model was chosen based on interaction geometry with the catalytic triad.

To consider additional side-chain conformation changes and subtle backbone movements upon binding, the complex structure generated by *Autodock Vina* was further refined using GalaxyRefine [34, 38]. Among 24 models generated by GalaxyRefine, the model having best GalaxyDock BP2 Score [39] was selected as the final model.

2.7 Site-directed Mutagenesis

Site-directed mutagenesis was performed using the QuickChange kit (Stratagene, CA, USA), and results were confirmed by DNA sequencing. The introduction of single site mutations into Est-Y29 was achieved by the use of pQE30-Est-Y29 as a template together with the primer sets described in Table 2. Bold nucleic acids with underlines in primer sequences indicate the codon or anticodon of a mutant. Mutagenesis at each site was performed using polymerase chain reaction (PCR). Briefly, after initial activation of *Pfu* polymerase (Cosmo Genetech, Korea) at 368 K for 5 min, 15 repeats of the cycle including denaturation at 368 K for 30 s, annealing at 328 K for 30 s, and extension at 345 K for 12 min, followed. Then, an extra extension was given at 345 K for 15 min, and the product was stored at 277 K. To separate the parental template from the mutated template, the product was incubated with 10 unit of *DpnI* (New England Biolabs, MA, USA) at 310 K for 1 h before being transformed into competent *E. coli* XL1-Blue cells. Colonies positive to 50 $\mu g \cdot mL^{-1}$ ampicillin were selected, and sequences of extracted plasmid were identified.

Table 2. Primer Information to Generate Est-Y29 Mutants

Mutation	Sequence
F125W	
Forward	5′-G GCT GGC TTT TCA TAT GAT **TGG** TCG TTG GGA TGC CC-3′
Reverse	5′-GG GCA TCC CAA CGA **CCA** ATC ATA TGA AAA GCC AGC C-3′
R225A	
Forward	5′-GAA GTG TAC GGA ATG **GCG** TCT CTT CAC GGA CTG-3′
Reverse	5′-CAG TCC GTG AAG AGA **CGC** CAT TCC GTA CAC TTC-3′
A348V	
Forward	5′-TTC GGT TGG AGC GGA **GTC** GCA GCA ACA TAT TTT-3′
Reverse	5′-AAA ATA TGT TGC TGC **GAC** TCC GCT CCA ACC GAA-3′

2.8 Thermal stability assay

Thermo-stabilities of the wild-type and F125W Est-Y29 were tested using circular dichroism (CD) spectroscopy (Jasco, Easton, MD, USA). Both the wild-type and mutant Est-Y29 were prepared as previously described at the concentration of 50 μM in the buffer containing 20 mM

phosphate pH8.0. Wavelength was scanned from 190 nm to 250 nm at 297 K, and the optimal point was selected at 217 nm, which showed the absolute maximum value in helical structure. Thermostability was tested at 217 nm by increasing the temperature from 283 K to 363 K. Results were analyzed by three-segment linear equation, and the melting temperature (T_m) was calculated by average value of interaction points between two etquations. Each sample was measured in triplicate and statistically analyzed using *Student*'s T-test. To measure the stability of the wild-type and mutant Est-Y29 in the presence of substrates, Est-Y29 at the concentration of 50 μM was mixed with 400 μM of (*S*)-ketoprofen ethyl ester or (*R*)-ketoprofen ethyl ester, and their T_m values were determined by monitoring the ellipticity change at 246 nm in the temperature ranges from 323 K to 363 K. Due to noise at the high energy wavelength possibly caused by the presence of DMSO in the buffer, ellipticity change was monitored at 246 nm.

2.9 Activity Assays

To test functional thermostability, Est-Y29 were prepared after heat exposure. Est-Y29 was incubated in various temperature points from 308 K to 363 K for 30 min, and was cooled down at 298 K for 10 min. For analysis of residual hydrolysis activity, initial velocity of hydrolysis of *p*-nitrophenol butyrate (*p*-NB) was measured by chasing color change at 405 nm wavelength time-dependently. Residual enantioselective catalytic activity of Est-Y29 was also verified using (*R*)- and (*S*)-Roche ester (methyl 3-hydroxy-2-methylpropionate) as substrates through color change of pH indicator, phenol red, and color change was measured at 430 nm wavelength time-dependently. Each reaction was repeated 3-4 times, and its initial velocities were averaged.

Enzyme reactions were preceded with 1 mM racemic ketoprofen ethyl ester in 10 mM Tris-HCl buffer pH 8.0 at 323 K. Conversion ratio of racemic ketoprofen to initial racemic ketoprofen ethyl ester was measured using NMR. The products, (*R*)- and (*S*)-ketoprofen, were

analyzed using a chiral compound analytical column, Chirex Phase 3005 (Phenomenex Co., CA, USA) mounted on HPLC (Agilent, CA, USA) and UV detector at 254 nm. The mobile phase contained 0.03 M ammonium acetate and 70% methanol. To obtain appropriate *E* value, conversion ratio was controlled to be less than 0.5. Enantiomeric excess of product (ee_P), conversion (c), and *E* value were calculated using the following equations:

$$ee_P = (C_S - C_R)/(C_S + C_R)$$

$$c = (C_S + C_R)/C_{e0}$$

$$E = \ln[1-c(1+ee_P)]/\ln[1-c(1-ee_P)]$$

where C_S and C_R represent concentrations of *(S)*-ketoprofen and (*R*)-ketoprofen, respectively, in the hydrolyzed products, and C_{e0} represents the initial concentration of substrate racemic ketoprofen ethyl ester in the hydrolysis reaction.

2.10 Enzyme Kinetic Analysis

Enzyme kinetic parameters of the wild-type and F125W Est-Y29 were obtained by measuring the rate of hydrolysis of either the pure (*R*)- or (*S*)-ketoprofen ethyl esters at various substrate concentrations at 323K for 5-10 min, which was in the range of initial rates, in 50 mM Tris-HCl buffer (pH 8.0). The enzyme concentration was 0.3 $mg \cdot mL^{-1}$. The reaction rate was determined by comparing the amount of product with the residual reactant at the time of stopping reaction using high performance liquid chromatography (HPLC). Agilent 1260 Infinity HPLC system was used equipped with the column Chiralpak IC (4.6 mm x 250 mm). The eluent was 10 % IPA and hexane (0.1 % Trifluoroacetic acid), and the area of the peak observed under UV (254 nm) wavelength was used to determine the reaction rate. The enzyme kinetic parameters, K_m and V_{max} were determined using GraFit 7 (Erithacus Software, Surrey, UK).

3. Results

3.1 Structural Studies of Est-Y29 in Complex with (*S*)-Ketoprofen

To explain the binding mode and selectivity of Est-Y29 for the *S*-enantiomer, we attempted to identify the complex structure of Est-Y29 and (*S*)-ketoprofen ethyl ester by co-crystallizing the protein and the substrate under low pH conditions (pH 4.6). However, upon crystallization, we determined that we obtained the (*S*)-ketoprofen-bound structure of Est-Y29, named Est-Y29-SKP, instead of the (*S*)-ketoprofen ethyl ester-binding form (Figure 1A). Yoon *et al.* characterized the activity of Est-Y29 as below 20% under acidic conditions [23], and thus it is assumed that hydrolysis of (*S*)-ketoprofen ethyl ester occurs during incubation and crystallization. Although Est-Y29-SKP fails to directly reveal the ethyl substituent in the ester bond of (*S*)-ketoprofen ethyl ester, it still provides insight into the enzyme-substrate interactions through benzophenone and the chiral center of the *S*-enantiomer in the product complex.

The overall structure of the complex Est-Y29-SKP is very similar to the apo Est-Y29 structure (PDB 4P6B) with a root mean square deviation (RMSD) value of 0.13 Å for 2573 atoms out of all 2943 atoms in the Est-Y29 (residue 1-389) (Figure 1A). Atoms in the loop containing residues 225-230 were not included for RMSD calculation. In the apo-structure, the electron density map at the loop 225-230 in Est-Y29 is poorly defined, which suggests that this loop is more flexible in the absence of ligand. In the Est-Y29-SKP structure, two residues in this loop, R225 and L227, interact directly with the phenol group of the (*S*)-ketoprofen (Figure 1A). The substrate position in the binding pocket can be stabilized due to the movement and interaction of the flexible loop 225-230 with the substrate. Thus, the volume of the pocket in Est-Y29 shows a difference between the apo and (*S*)-ketoprofen-binding forms (Figure 1B). The electron density map $2F_O$-F_C of (*S*)-ketoprofen is clearly defined in the active site of Est-Y29-SKP (Figure 1C). This suggests that (*S*)-ketoprofen locates in a substrate-binding pocket of Est-Y29 with high occupancy. (*S*)-ketoprofen is stabilized in the binding site of Est-Y29 by

numerous favorable interactions. In detail, binding of (*S*)-ketoprofen occurs by direct hydrogen bonds of (*S*)-ketoprofen with main-chain S58 (3.1 Å) and A348 (3.0 Å), which form the oxyanion hole and the catalytic S58 (Figure 1D). Furthermore, the oxygen in the benzophenone group makes a water-mediated hydrogen bond with residue Y57 and S248, and many π interactions help to hold the benzophenone of (*S*)-ketoprofen. Specifically, residues R225, L227, and L370 stabilize one phenyl group of (*S*)-ketoprofen, while residues Y57, I141, H261, and A348 interact with the other phenyl group via various π-σ, π-cation, π-π, and π-alkyl interactions (Figure 1E). Importantly, the methyl substituent at the chiral carbon center makes three π-alkyl interactions with residues Y123, F125, and Y170 with the distances of 4.4, 4.6 and 5.1 Å, respectively. These aromatic interactions explain why Est-Y29 has a preference for the (*S*)-ketoprofen ethyl ester.

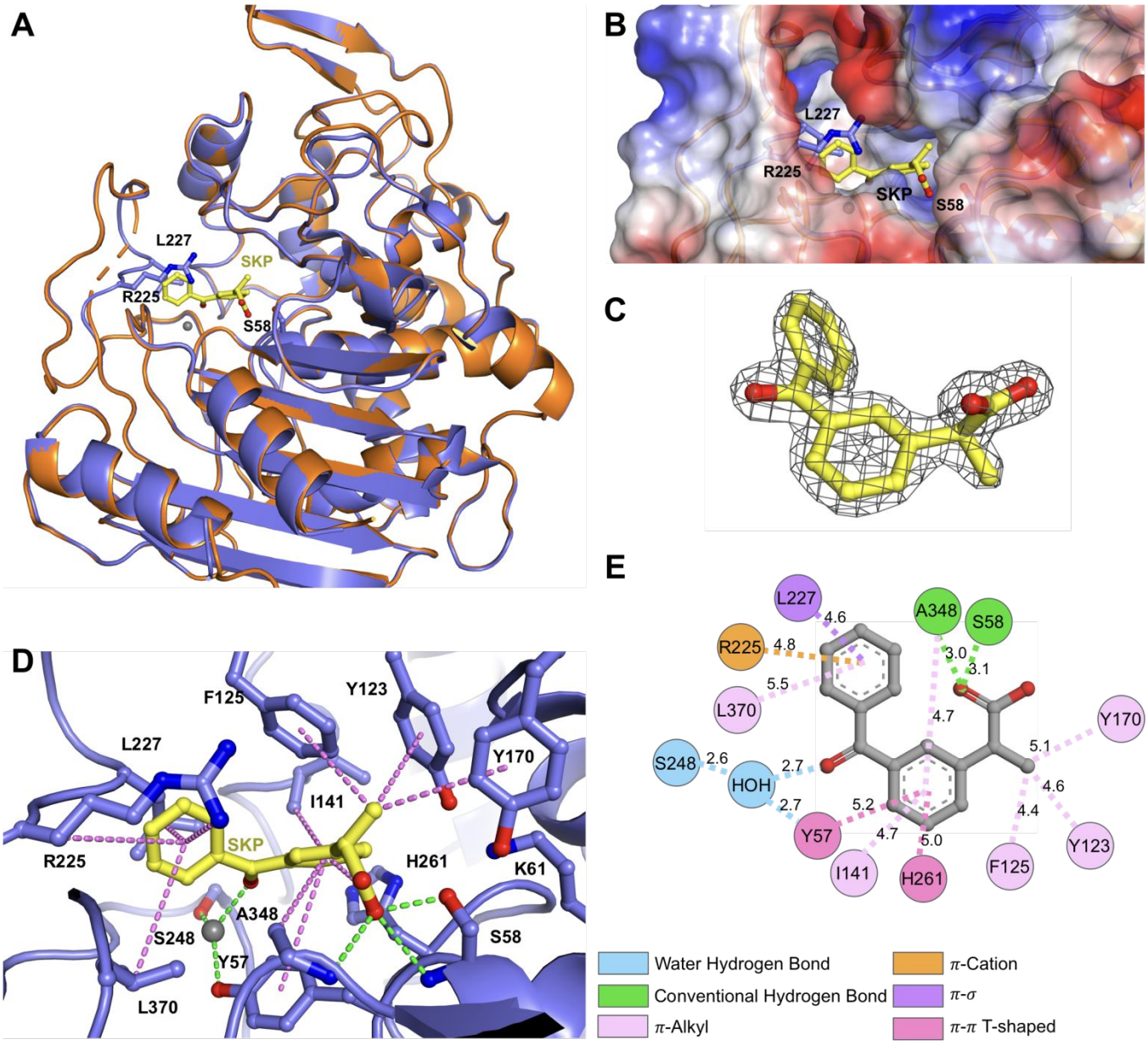

Figure 1. Complex Structure of the Est-Y29 with (*S*)-Ketoprofen. (A) Superimposition of the apo Est-Y29 (orange cartoon representation, PDB ID: 4P6B) and the complex Est-Y29 with (*S*)-ketoprofen (slate cartoon representation). (*S*)-ketoprofen is shown in yellow in the stick representation. Specific residues on the flexible loop 225-230 are shown in the slate stick representation. The dashed tube represents the missing residues in the apo Est-Y29 structure. (*S*)-ketoprofen is marked as SKP in the figure. (B) Surface representation colored by the vacuum electrostatic potential of apo Est-Y29 in the same orientation as in (A). (C) $2F_O$-F_C map contoured at 1.5 σ shows clear electron density for (*S*)-ketoprofen, shown in yellow stick representation. (D) Detailed interactions of (*S*)-ketoprofen (yellow sticks) and residues in the active site of Est-Y29 (slate stick representation). The water molecule involved in substrate

binding is shown as grey sphere. Hydrogen bonds are indicated with green dashed lines. π interactions (π-cation, π-σ, π-π, and π-alkyl) are shown with violet dashed lines. S58 is the catalytic residue. An oxyanion hole is formed by the main chain NH of S58 and A348. (E) 2D ligand interaction diagram of (*S*)-ketoprofen with the Est-Y29 active site. Atomic interactions are indicated by the dotted lines and their distances in angstroms are shown.

3.2 Docking Simulation of Est-Y29 with (*R*)- and (*S*)-Ketoprofen Ethyl Ester

To get insight into the enantioselectivity of Est-Y29, we performed induced-fit docking studies of each substrate, (*S*)- and (*R*)-ketoprofen ethyl esters, separately. We used the crystal structures of Est-Y29-SKP a template for the docking study after removing (*S*)-ketoprofen and glycerol. For the induced-fit docking analysis, key residues involved in ligand binding were allowed for flexible movement during docking. Then, the docking models were further refined using GalaxyRefine[34, 38], which is used for iterative sidechain repacking and the relaxation of the overall structures. The induced-fit docking approach used in this study was successfully validated in the previous study of the GPCR-ligand docking [40].

The induced-fit docking models show that (*S*)-ketoprofen ethyl ester binds to the pocket occupied by (*S*)-ketoprofen in the crystal structure of Est-Y29-SKP, suggesting that the docking was successful. In addition, the docking model was validated by that the carbonyl oxygen of the (*S*)-enantiomer makes hydrogen bonds with oxyanion hole formed by the NH of S58 (3.4 Å) and A348 (2.9 Å), (Figure 2A). Residues L227, R225, L370, and A348 stabilize the benzophenone group by π-alkyl interactions (Figure 2B). F125 and Y123 also stabilize benzophenone group by π-π interactions. The methyl substituent at the chiral center makes a π-alkyl interaction with residues Y123, F125, and Y170 at distances of 5.5 Å, 4.3 Å and 5.2 Å, respectively (Figure 2A). When the active site of the docking model of Est-Y29-SKE is superimposed over the crystal structure Est-Y29-SKP, two ligands ((*S*)-ketoprofen and (*S*)-ketoprofen ethyl ester) occupy the same position, and the key interactions in both structures are well conserved (Figure S2A), thus verifying the accuracy of the docking model of Est-Y29-

SKE. The docking model of Est-Y29 with (*R*)-ketoprofen ethyl ester (Est-Y29-RKE) also binds Est-Y29 in a productive mode (Figure 2C), in which the carbonyl oxygen forms hydrogen bonds with S58 (3.4 Å) and A348 (2.8 Å). Key residues stabilizing the benzophenone group of (*R*)-ketoprofen ethyl ester by π-interactions include I141, L227, L370, H261, and A348 (Figure 2D). The residues stabilizing the benzophenone and carbonyl oxygen of the ligands are highly conserved between the two docking structures. Superimposing the docking model Est-Y29-RKE onto the crystal structure of Est-Y29-SKP suggests that the binding mode of the docking (*R*)-ketoprofen ethyl ester and (*S*)-ketoprofen in the active site of Est-Y29 are similar (Figure S2B). The most pronounced difference between the RKE- and SKE-bound docking models lies on the opposite orientation of CH_3 and H substituents in the chiral center (Figure S2C). Instead of interacting with the aromatic pocket formed by residues Y123, F125, and Y170, the methyl substituent of (*R*)-ketoprofen ethyl ester forms π-alkyl and alkyl interactions with the nearby residues A348 and F125 (Figure 2C).

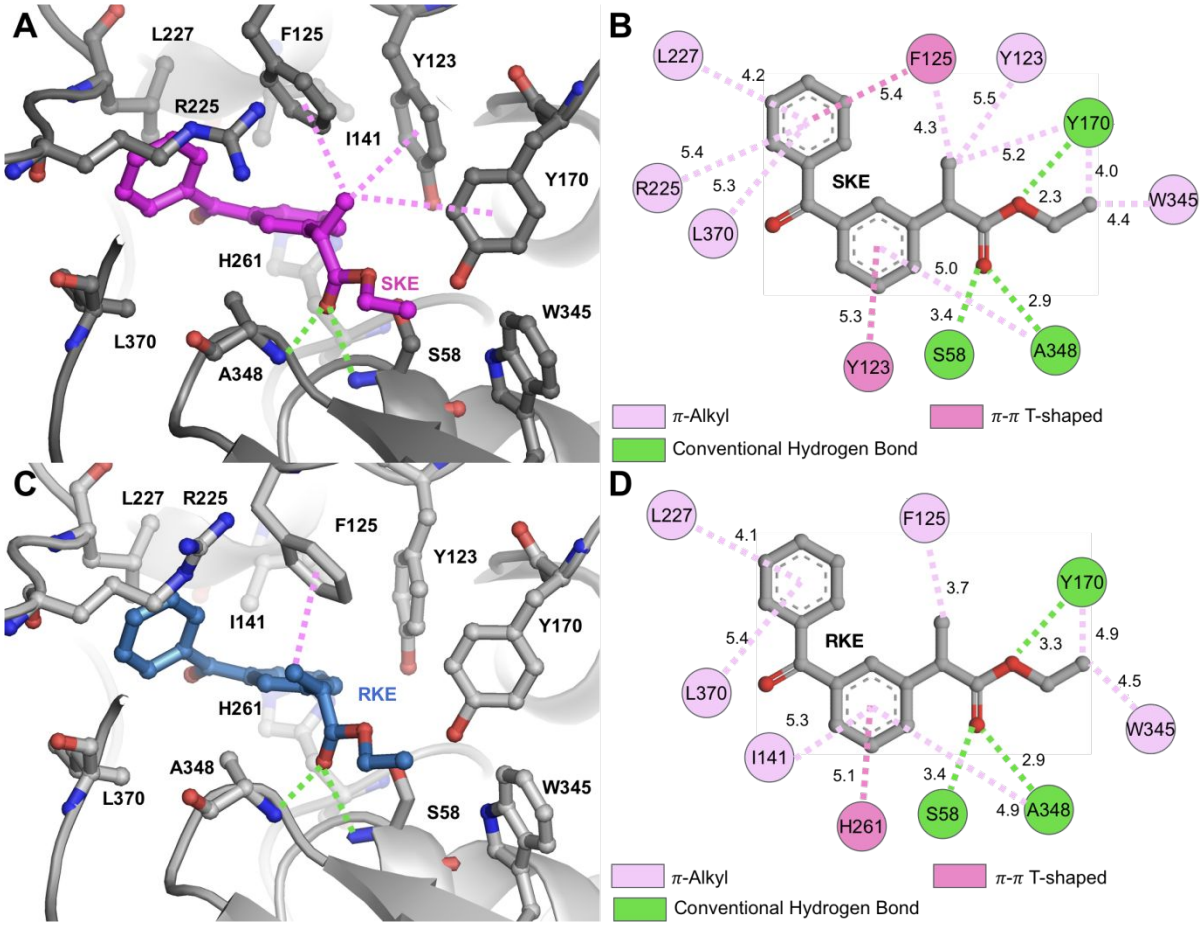

Figure 2. Docking Models of (*R*)- and (*S*)-Ketoprofen Ethyl Ester to Est-Y29

(A) Detailed interactions of the docking (*S*)-ketoprofen ethyl ester (magenta sticks) and residues in the active site of Est-Y29 (grey stick representation). Hydrogen bonds are indicated with green dashed lines. π–interactions (π-π, and π-alkyl) are shown with violet dashed lines. (*S*)-ketoprofen ethyl ester is marked as SKE in the figure. (B) 2D ligand interaction diagram of docking (*S*)-ketoprofen ethyl ester with the Est-Y29 active site. (C) Detailed interactions of the docking (*R*)-ketoprofen ethyl ester (marine sticks) and residues in the active site of Est-Y29 (grey stick representation). Hydrogen bonds are indicated with green dashed lines. π–interaction is shown with violet dashed lines. (*R*)-ketoprofen ethyl ester is marked as RKE in the figure. (D) 2D ligand interaction diagram of docking (*R*)-ketoprofen ethyl ester with the Est-Y29 active site. In Figures (B) and (D), atomic interactions are indicated by the dotted lines and their distances in angstroms are shown.

3.3 Structure-based Design of Est-Y29 Mutants

The crystal structure of the complex Est-Y29-SKP together with docking results suggest that binding of two substituents CH_3 and H at the chiral center of (*S*)-ketoprofen ethyl ester plays a major role determining Est-Y29 enantioselectivity; therefore, residues far away from these two substituents are likely not good targets for mutagenesis. To test this hypothesis, we designed a mutation at residue R255A to abolish the π-cation interaction between the R255 to the phenyl group of (*S*)-ketoprofen ethyl ester. Although residue R255 interacts directly with the ligand, it does not contribute to the binding of these two substituents. As we expected, mutation R255 did not affect the enantioselectivity since R255A showed a similar *E* value to the wild-type enzyme (Table 3).

Since the aromatic pocket interacts directly with the CH_3 substituent of (*S*)-ketoprofen ethyl ester, it is expected that binding affinity of the (*S*)-enantiomer to protein can be enhanced by increasing π-interaction. As we expected, when replacing F125 to W, the *E* value increased from 4.48 to 20.39 (Table 3). Together with the approach to increase the binding of the (*S*)-enantiomer, we designed another mutant that has reduced binding affinity to (*R*)-enantiomer. The distance from chiral center in substrate to side chain Cβ in A348 is 3.7 Å, and the distance between Cα in A348 and CH_3 substituent in (*S*)-substrate is 4.4 Å. The docking models revealed that Cβ atom in A348 is closer to the CH_3 substituent of (*R*)-ketoprofen ethyl (3.7 Å) than that of (*S*)-ketoprofen ethyl ester (5.1 Å) (Figures 2 and S2). Accordingly, it is expected that replacing A348 with a bulkier side chain residue would increase the repulsion force to the (*R*)-ketoprofen ethyl ester substrate, which makes the binding preference to (*R*)-ketoprofen ethyl ester smaller. Therefore, we expected that a mutation at A348 would lead to higher enantioselectivity by preventing the binding of the *R*-enantiomer to the active site of Est-Y29. Surprisingly, the mutant A348V showed no enantioselectivity (Table 3).

Table 3. Enantioselectivity Values of Est-Y29 and Its Mutants toward (*S*)-Ketoprofen[a].

protein	conversion	ee_P	*E* value
Est-Y29	0.4045	0.5245	4.48
Est-Y29 R225A	0.5339	0.4823	4.84
Est-Y29 A348V	0.4686	0.3760	1.11
Est-Y29 F125W	0.3598	0.8540	20.39

[a] Representative HPLC analysis results are described in Figure S3.

3.4 Crystal Structure of A348V-SKE

To explain the poor enantioselectivity of mutant Est-Y29 (A348V) toward (*S*)-substrate selectivity, we solved the crystal structure of the mutant A348V with its substrate (*S*)-ketoprofen ethyl ester using a co-crystallization approach. In this structure, we observed the clear electron density of the ester substrate but not the hydrolyzed product (Figure 3A). Unlike expectation from docking models, the longer and bulkier A348V residue was not stretched out to the chiral center of the substrate, and eventually failed to bring direct hindrance in the space for the methyl substituent in the chiral center of the (*R*)-ketoprofen ethyl ester. Rather, there were less favorable interactions of substrate (*S*)-ketoprofen ethyl ester with the mutant Est-Y29 A348V. Two phenyl groups of the (*S*)-ketoprofen ethyl ester were stabilized by π-interactions with residues Y57, I141, F125, H261, and V348. The oxygen of the benzophenone group makes a water-mediated hydrogen bond with residue Y57 and S248, but there is no hydrogen bond between (*S*)-ketoprofen ethyl ester and the oxyanion hole (V348 and S58) as was observed in the Est-Y29-SKP crystal structure (Figures 3B and C). When compared to (*S*)-ketoprofen bound to Est-Y29, the (*S*)-ketoprofen ethyl ester in A348V occupies a similar position to the active site, but the methyl substituent at the chiral center of (*S*)-ketoprofen ethyl ester does not make a π-alkyl interaction with the aromatic pocket formed by F125, and Y170 (Figure 3D). Instead, this methyl group make π-alkyl interactions with residues Y123 and H261.

We assume that, due to the unfavorable orientation of (*S*)-ketoprofen ethyl ester in A348V, the mutant shows no preference for the *S*-enantiomer.

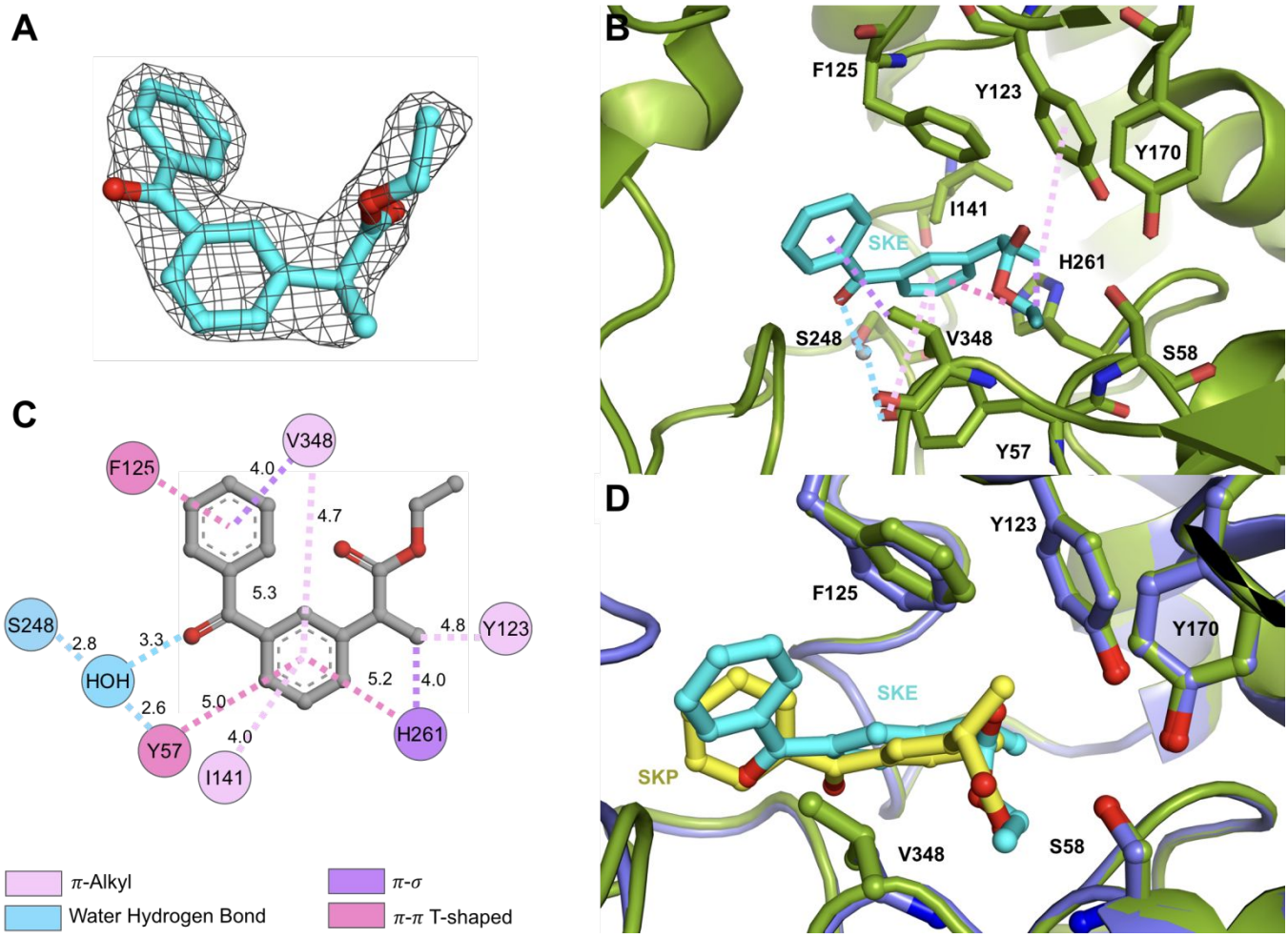

Figure 3. Structure of the Mutant Est-Y29 (A348V) Bound to (*S*)-Ketoprofen Ethyl Ester

(A) $2F_O$-F_C map contoured at 1.0 σ shows clear electron density for (*S*)-ketoprofen ethyl ester, shown in cyan in the stick representation. (B) Detailed interactions of (*S*)-ketoprofen ethyl ester (cyan sticks) and residues in the active site of the mutant Est-Y29, A348V (split pea stick representation). The water molecule involved in SKP binding is shown as grey sphere. Hydrogen bonds are indicated with green dashed lines. π interactions (π-σ, π-π, and π-alkyl) are shown with violet dashed lines. (C) 2D ligand interaction diagram of (*S*)-ketoprofen ethyl ester with the active sites of the mutant A348V. Atomic interactions are indicated by the dotted lines and their distances in angstroms are shown. (D) Superimposition of the residues in the active sites of Est-Y29-SKP (slate sticks) and A348V-SKE (split pea sticks) shows the difference of orientation of the methyl group at the chiral center. (*S*)-ketoprofen is shown with yellow sticks while (*S*)-ketoprofen ethyl ester is shown as cyan sticks.

3.5 Crystal Structure of the Mutant Est-Y29, F125W

In an attempt to explain the increased enantioselectivity of the mutant Est-Y29 (F125W), we tried to solve the structure of the mutant protein with (*S*)-ketoprofen ethyl ester. However, despite extensive efforts, we failed to obtain the complex structure. We therefore crystallized the apo-mutant Est-Y29 F125W in order to examine the aromatic pocket. In this structure, we observed the different conformation of the loop 225-230, which contains two residues R225 and L227 responsible for interacting with the ketoprofen substrates (Figure 4A). In the apo-Est-Y29, this loop is missing, possibly due to its flexible nature. Since R225 and L227 contribute to the ligand binding, loop 225-230 becomes ordered when the ligand is introduced, as seen in the structure Est-Y29-SKP and A348V-SKE. In the crystal structure of Est-Y29 F125W, although there is no ligand, R225 makes a strong π-cation interaction with W125. Therefore, loop 225-230 is still ordered even in the absence of ligand (Figure 4A). However, residues 225-227 are located close to the product or substrate binding site in the Est-Y29-SKP or A348V-SKE.

We also noticed that residue W125 of F125W shows similar orientation to F125 of Est-Y29-SKP (Figure 4B). For the quantitative analysis of the substrate binding sites in the wild-type and F125W, their cavity volumes were calculated. The results showed that volumes of the wild-type and F125W Est-Y29 are 1240A^3, and 582 A^3, respectively. The difference in the volume of each structure is mostly due to the structural change in the loop (R225-L230) (Figure 4). For example, in the case of F125W, the residues 225-227 occupied the substrate binding sites; accordingly, the volume of active site cavity is the smallest. For the comparison between the wild-type and F125W mutant, we made a model of F125W by changing F125 into tryptophan residue followed by energy minimization, using the wild-type structure as a template. The cavity volume of this model is 711 A^3, 40% less than the volume of the wild-type Est-Y29. The volume in the mutant cavity is reduced because W125 closes the hole to the

smaller pocket (Figure. S4).). Although the cavity volume has been changed, it is noteworthy that the size of the substrate binding pocket seems to be not changed since the smaller pocket is not involved in the substrate binding, suggesting that substrate binding is not affected by the mutation at F125. From this analysis, it is expected that the area of the hydrophobic surface that interacts with the alkyl moiety of substrate has been increased in F125W since the area corresponding to the door of the hole to the extra-pocket is covered by the tryptophan residue (Figure S4), which implies that F125W might have the enhanced binding affinity to the substrate in comparison to the wild-type enzyme.

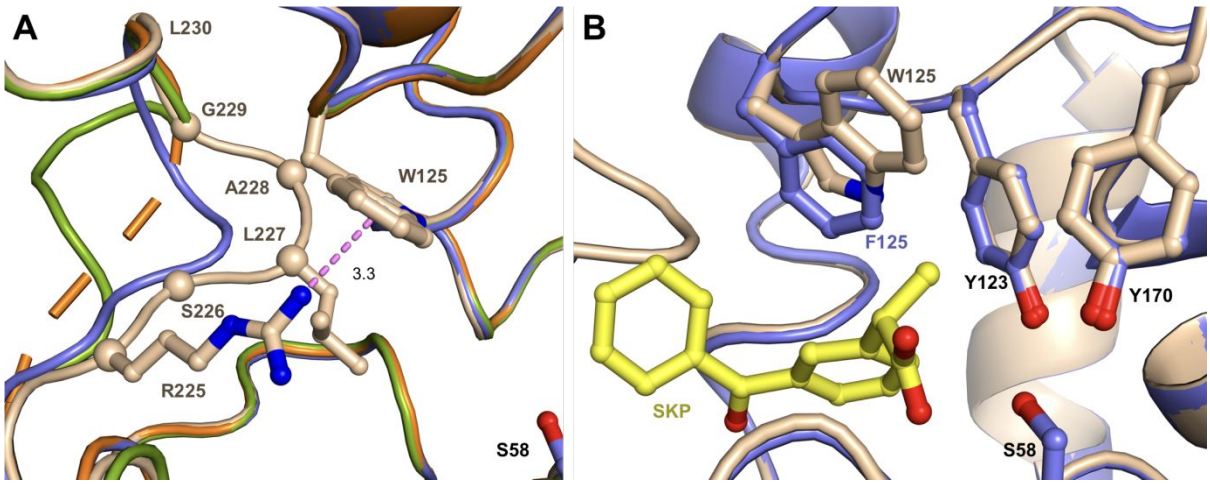

Figure 4. Superimposed Active Site Structures of Est-Y29

(A) Superimposition of apo Est-Y29 (orange cartoon), Est-Y29-SKP (slate cartoon), Est-Y29 A348V-SKE (split pea cartoon), and Est-Y29 F125W (wheat cartoon) show multiple conformations of the loop 225-230. Residues from 225 to 230 are shown as spheres. The π-cation interaction between R225 and W125 in Est-Y29 F125W is shown as violet dashed lines. Distances in angstroms between the center of aromatic ring of W125 and a guanidinyl group of R225 is shown. (B) Superimposition of residues in the active sites of Est-Y29-SKP (slate sticks) and Est-Y29 F125W (wheat sticks) shows that the aromatic pocket formed by Y123, W125, and Y170 in Est-Y29 F125W is commonly conserved in the wild-type and F125W Est-Y29 structures. (*S*)-ketoprofen of Est-Y29-SKP is shown as yellow sticks.

3.6 Kinetic Studies of the Wild-Type and F125W Est-Y29

To understand the enhanced enantioselectivity of the mutant F125W, we measured enzyme kinetic parameters of the wild-type and F125W EST-Y29 with two substrates (*R*)- and (*S*)-ketoprofen ethyl ester (Figure 5 and Table S1). It can be seen that the catalytic efficiency (k_{cat} /K_M) of F125W was 4-fold higher for (*S*)-ketoprofen ethyl ester than for (*R*)-ketoprofen ethyl ester, which is improved from 1.7-fold higher catalytic efficiency for (*S*)-ketoprofen ethyl ester in the wild-type enzyme. Moreover, the catalytic efficiency of F125W for (*S*)-ketoprofen ethyl ester was in fact improved 1.4-fold from the wild-type enzyme while the catalytic efficiency of F125W for (*R*)-ketoprofen ethyl ester was worsened 1.8-fold from that of the wild-type Est-Y29. This clearly shows that the enhanced enantioselectivity actually comes with the comparable or enhanced catalytic efficiency for the (*S*)-enantiomer as well as the significantly decreased catalytic efficiency for the (*R*)-enantiomer.

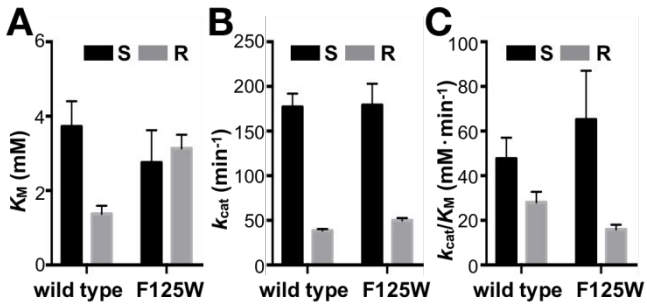

Figure 5. Kinetic Analysis of the Wild-Type and F125W Est-Y29 to (*R*)- and (*S*)-Ketoprofen Ethyl Esters. (A) K_M of the wild-type and F125W Est-Y29 to (*S*)-ketoprofen ethyl ester (black bar) and (*R*)-ketoprofen ethyl ester (gray bar). (B) k_{cat} of the wild-type and F125W to (*S*)-ketoprofen ethyl ester (black bar) and (*R*)-ketoprofen ethyl ester (gray bar). (C) Catalytic efficiency k_{cat}/K_M of the wild-type and F125W Est-Y29 to (*S*)-ketoprofen ethyl ester (black bar) and (*R*)-ketoprofen ethyl ester (gray bar). For fitting on Michaelis-Menten equation, 5-8 points of substrate concentrations were used. Catalytic efficiency was obtained from division of k_{cat} by K_M. Graphs were drawn using the values in Table S1.

3.7 Functional Improvement of Engineered Est-Y29

The wild-type Est-Y29 presented high thermostability with marginal enantioselectivity, which is an attractive characteristic for industrial application [23]. In this study, we improve the enantioselectivity of Est-Y29 by mutating Phe at 125th residue to Trp by five-fold increasing the *E* value toward the (*S*)-ketoprofen ethyl ester compared with the wild-type enzyme. For industrial applications, it is necessary to test the stability and hydrolysis activity of the mutant in comparison with the wild-type enzyme. The T_m values of the wild-type and the mutant are quite similar (344.6 K for the wild-type and 345.6 K for the mutant F125W), suggesting that replacement of F125 to W125 does not alter the protein stability (Figure 6A). However, mutant F125W showed lower residual activity than the wild-type protein after incubation at higher temperature conditions (Figure 6B). Therefore, we further investigated whether the substrate affects the stability of the enzyme by measuring Tm values in the presence of the saturating amount of substrates, (*S*)- and (*R*)-ketoprofen ethyl ester. However, we found that both enantiomers did not contribute the stability of enzymes since there was little Tm value change (Figure S5). Therefore, it is very likely that the lower activity of F125W at high temperature is caused not by the lower complex stability but by the lower catalytic activity.

When the Roche ester enantiomer was applied to characterize enantioselectivity of wild-type and mutant Est-Y29 (Figure 6C), we found that the residual enantioselectivity of mutant Est-Y29 did not change at high temperatures (Figure 6D). The ratio of activity to *S*- and *R*-form is sustained in overall temperature up to 338 K. Interestingly, unlike the ketoprofen ethyl ester, both activity and selectivity to the *S*-enantiomer of the wild-type Est-Y29 were higher than those of the mutant F125W when the Roche ester was used as a substrate. This result can be explained by that F125W is designed to fit on (*S*)-ketoprofen ethyl ester by strengthened aromatic environment at benzophenone group and chiral center. Thus, the mutation is not fatal and does not destroy intramolecular interactions, pocket structure, and

selective function, but it does increase its targeted enantioselectivity to *S*-enantiomer of ketoprofen ethyl ester.

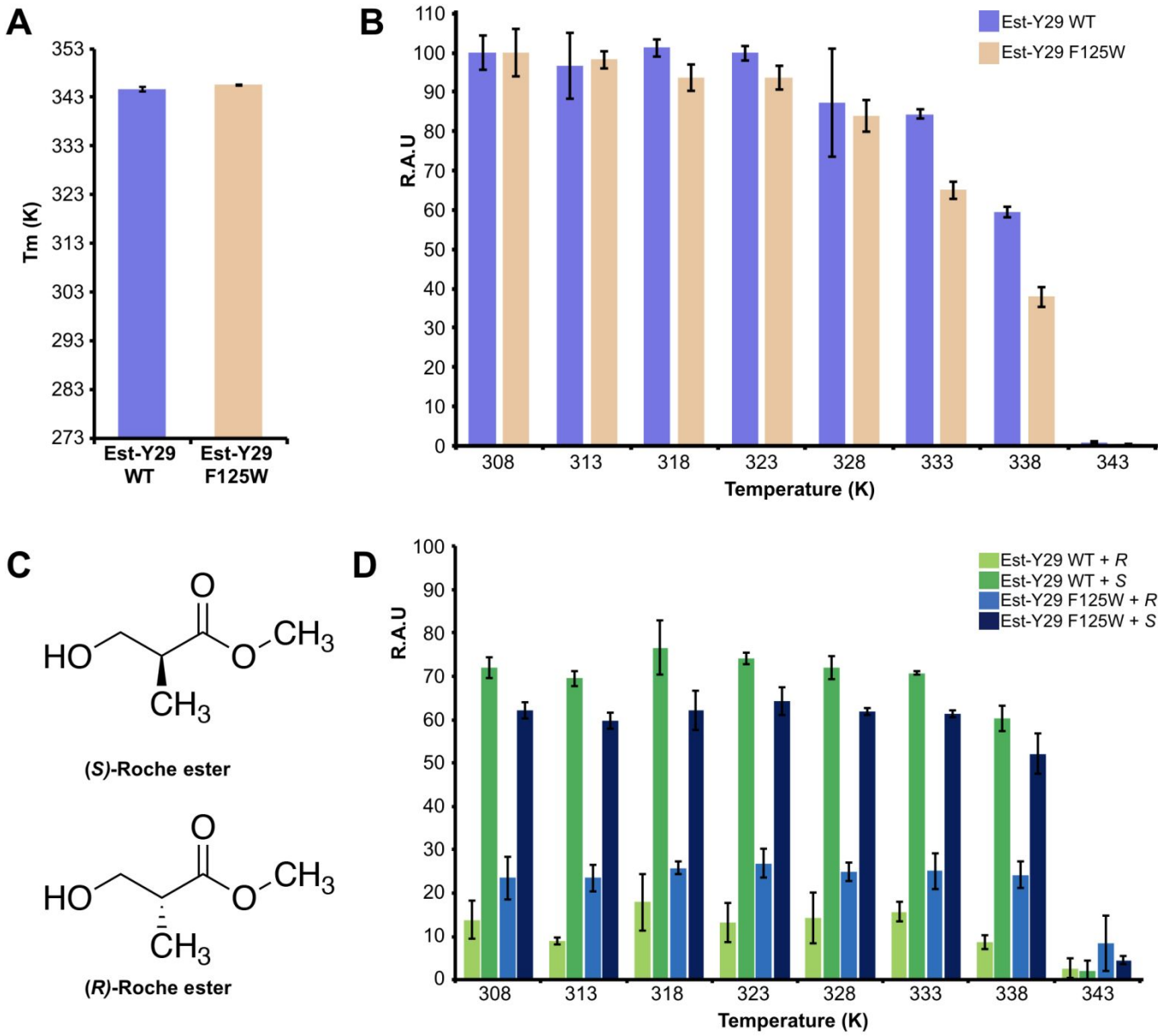

Figure 3. Thermal Stability and Enantioselectivity of the Wild-Type and F125W Est-Y29. (A) Thermal melting points of the wild-type (Est-Y29 WT) and mutant Est-Y29 (Est-Y29 F125W) obtained by circular dichroism (CD) analysis. (B) Residual activity of the wild-type and F125W Est-Y29 at different temperature conditions. (C) Chemical structures of (*R*)- and (*S*)-Roche ester used in the enantioselectivity assay in (D). (D) Temperature dependent change in the enantioselectivity of the wild-type and F125W Est-Y29.

4. Discussion

In this study, we solved the crystal structures of the thermostable Est-Y29 in the product-bound form and its mutant in substrate-bound form. From the structural analysis, combining with docking studies of Est-Y29 with both (*R*)- and (*S*)-ketoprofen ethyl ester, we explained the molecular basis of enantioselectivity toward the (*S*)-ketoprofen ethyl ester. We found that Y123, F125, and Y170 create an aromatic pocket that is involved in the π-alkyl interaction with the methyl substituent of (*S*)-ketoprofen. Accordingly, the mutants F125W showed higher enantioselectivity with five-fold enhanced enantioselectivity compared to the wild-type Est-Y29 due to the increased π-interaction.

In addition, by kinetic analyses, we showed that F125W mutation decreased K_M for (*S*)-ketoprofen ethyl ester 1.3-fold, in comparison to the wild-type enzyme, while the same mutation increased K_M 1.8-fold for (*R*)-ketoprofen ethyl ester. This suggests the F125W mutation created a higher substrate binding affinity for (*S*)-ketoprofen ethyl ester, while it decreased the binding affinity for (*R*)-ketoprofen ethyl ester compared to the wild-type Est-Y29. On the other hand, the wild-type Est-Y29 and F125W showed similar values of k_{cat}. These changes led to a 4-fold higher catalytic efficiency ($k$cat/K_M) of F125W for (*S*)-ketoprofen ethyl ester than for (*R*)-ketoprofen ethyl ester. Hence, it is highly likely that the changes in binding affinity, mainly the decreased binding affinity for R-substrate, is a major driving force in the higher enantioselectivity of F125W in favor of the S-form ketoprofen ester. Taking these together, we can propose that the enantioselectivity of Est-Y29 comes from the difference in binding affinity rather than the transition state structure that is represented by the k_{cat} value.

Consistently, our docking analyses suggest that F125W has the higher binding affinity to the (*S*)-conformer since the docking scores of (*S*)-ketoprofen ethyl ester bound to the mutant Est-Y29 is higher than that of (*R*)-ketoprofen ethyl ester while scores for (*R*)-conformer is

higher in the case of the wild-type Est-Y29 (Table S2). In the structural aspect, this binding affinity change can be explained by the π-interaction change. Superposition of docking models of (*R*)- and (*S*)-ketoprofen ethyl ester substrates bound to Est-Y29 revealed that the first priority group ($COOC_2H_5$) and the second priority group (PheCOPhe) in the chiral center are positioned in a similar space, but the position of remaining substituents CH_3 and H are exchanged (Figure 7). For faster reacting (*S*)-ketoprofen ethyl ester, the substituent CH_3 lies close to the aromatic pocket formed by Y123, F125, and Y170, and the substituent H is closed to the side chain of F125 and A348. However, the substituent H is located in the aromatic pocket in the slower-reacting (*R*)-ketoprofen ethyl ester structure, creating two mismatches (Figure 7B). Docking models of F125W to (*S*)-ketoprofen ethyl ester (F125W-SKE) and (*R*)-ketoprofen ethyl ester (F125W-SKE) also support this view (Figure S6). Although the docking models of F125W are not identical to those of the wild-type enzyme, the closer distance of a benzophenone ring and chiral center in (*S*)-ketoprofen ethyl ester to W125 than those in (*R*)-ketoprofen ethyl ester is consistently found in the docking models of the wild type Est-Y29 (Figure 2). Trp was found as the greatest enrichment in the carbohydrate-binding pockets. Electron-rich aromatic Trp is the most likely residue to engage in the CH-π interactions [41], which enhances the (*S*)-ketoprofen ethyl ester-binding to Est-Y29 by increased binding affinity between the pocket and methyl group in the substrate.

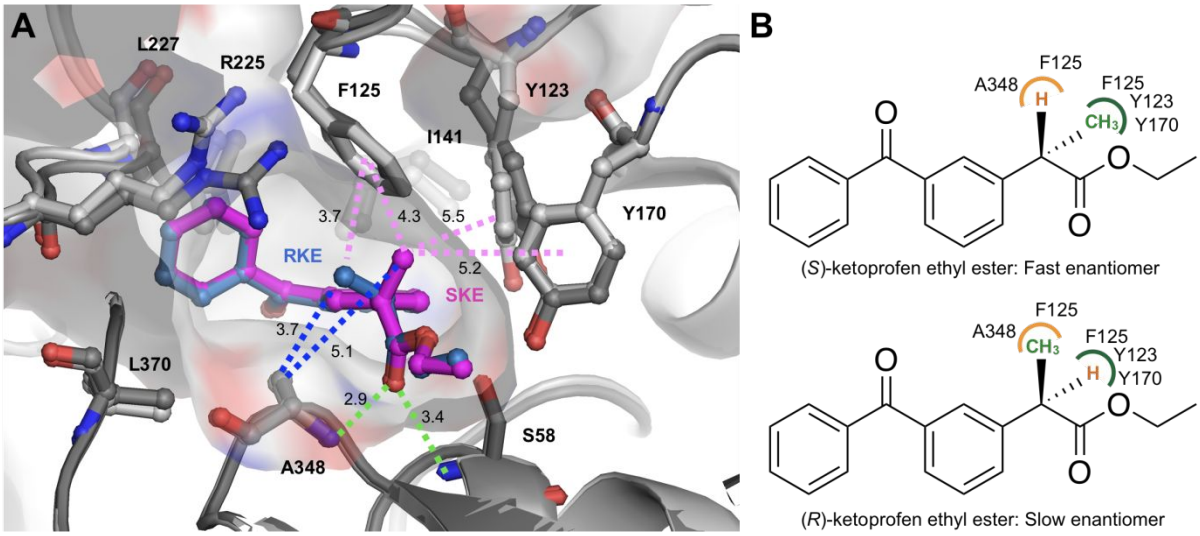

Figure 4. Structural Basis of Enantioselectivity of Est-Y29 toward (*S*)-Ketoprofen Ethyl Ester

(A) Superimposition of the docking models of (*R*)- and (*S*)-ketoprofen ethyl ester. (*S*)-ketoprofen ethyl ester is shown as magenta sticks while (*R*)-ketoprofen ethyl ester is shown as marine sticks. Important residues of Est-Y29 are shown as grey stick representation. Hydrogen bonds are indicated with green dashed lines. π-interactions (π-π and π-alkyl) are shown with violet dashed lines. (*R*)-ketoprofen ethyl ester and (*S*)-ketoprofen ethyl ester are marked as RKE and SKE, respectively. (B) Schematic of racemic (*R*,*S*)-ketoprofen ethyl ester in the active site of Est-Y29 in two possible configurations. The enantioselectivity originates from the different orientation of two substituents (H and CH_3) at the stereo-center of the ligands. The binding of (*S*)-ketoprofen ethyl ester is preferred due to the stronger π-alkyl interaction of the methyl group of (*S*)-ketoprofen ethyl ester to the aromatic pocket formed by Y123, F125, and Y170.

To enhance enzyme activity to a specific enantiomer, residues around substrate-binding site are regarded as effective targets. Especially, for enantioselectivity, the chiral center-positioned space in enzyme-substrate complex structures is an attractive area to regulate specificity to each enantiomer. By interfering with binding to the pocket and forming tetrahedral intermediates of unfavorable enantiomers, the enzyme allows desired enantiomers to approach and process them. To that end, we prepared A348V in which the V348 residue was

expected to clash with methyl substituent to chiral carbon in (*R*)-ketoprofen ethyl ester and repel it from the pocket. However, the replaced V348 forms additional π-alkyl interaction with the common benzophenone group in both the *R*- and *S*-enantiomers (Figure 3B), and increases especially the *R*-enantiomer binding by hydrophobic interaction instead of expected hindrance to the *R*-form. Moreover, distortion of ligand binding in A348V induced loss of interaction with residues for the oxyanion hole, and reduced stability of A348V to (*S*)-ketoprofen ethyl ester (Figure 4C). These were coincident with results of enantiomer analysis using HPLC as increase of activity to *R*-enantiomer and almost equal activity in both forms (Table 3).

In kinetic resolution, enantioselectivity of enzymes is also influenced by solution and temperature [42]. The racemic temperature (T_r) is a conceptual temperature, which makes enzymes produce both enantiomers equally at the T_r [43]. Jin *et al*. showed the temperature effect on enantioselectivity and increase or decrease of temperature from the T_r affected enantioselectivity [44]. Solution components such as detergent are also critical to determining *E* value [45]. In this study, we set the temperature to 323 K for selective hydrolysis in a fixed buffer. To improve enantioselectivity, the characterization of optimal conditions such as buffer and reaction temperature is additionally required to magnify endogenous enzyme selectivity. Therefore, we expect the enantioselectivity of F125W could be further enhanced by optimizing the reaction conditions, which is necessary for further industrial application of this enzyme. Furthermore, if F125W is used as a template for the directed evolution, Est-Y29 is expected to be engineered as a biocatalyst suitable for the industrial production of (*S*)-ketoprofen [464641]

Associated Content

Supporting Information

Substrate and product analyses data and docking model description (.pdf)

Crystallographic data (.cif) of Est-Y29-SKP (PDB code: 5ZWR), Est-Y29 F125W (PDB code: 5ZWV) and Est-Y29 A348V-SKE (PDB code: 5ZWQ)

This information is available free of charge on the ACS Publications website.

Author Information

ORCID

Tri Duc Ngo: 0000-0002-9599-0654

Changsuk Oh: 0000-0001-6347-1609

Kyeong Kyu Kim: 0000-0003-2515-8894

Corresponding Author

*To whom all correspondence should be addressed: Tel: 82-31-299-6136, Fax: 82-31-299-6159, E-mail: kyeongkyu@skku.edu

Author Contribution

$ These authors equally contribute this work.

KKK conceived and supervised the work. KKK, TDN, CO, WY, YR contributed to data interpretation. TDN, CO solved the crystal structure. TND, MP, CS performed the docking analysis, TDN, CO, PM, SL, KP, LN, HB, SBK, SY, BHR performed biochemical experiments. KKK, TDN, CO wrote the manuscript. All authors reviewed the final manuscript.

Funding Sources

This study was funded by National Research Foundation of Korea grants (2017M3A9E4078553) and the Next-Generation BioGreen 21 Program (SSAC-PJ01317301).

References

1. Sheldon, R. A.; Woodley, J. M., Role of Biocatalysis in Sustainable Chemistry. *Chem Rev* **2018,** 118, 801-38.

2. Bommarius, A. S.; Blum, J. K.; Abrahamson, M. J., Status of Protein Engineering for Biocatalysts: How to Design an Industrially Useful Biocatalyst. *Curr Opin Chem Biol* **2011,** 15, 194-200.

3. Bornscheuer, U. T.; Huisman, G. W.; Kazlauskas, R. J.; Lutz, S.; Moore, J. C.; Robins, K., Engineering the Third Wave of Biocatalysis. *Nature* **2012,** 485, 185-94.

4. Bordes, F.; Cambon, E.; Dossat-Letisse, V.; Andre, I.; Croux, C.; Nicaud, J. M.; Marty, A., Improvement of Yarrowia Lipolytica Lipase Enantioselectivity by Using Mutagenesis Targeted to the Substrate Binding Site. *Chembiochem* **2009,** 10, 1705-13.

5. Jaeger, K. E.; Reetz, M. T., Microbial Lipases Form Versatile Tools for Biotechnology. *Trends Biotechnol* **1998,** 16, 396-403.

6. Reetz, M. T.; Bocola, M.; Wang, L. W.; Sanchis, J.; Cronin, A.; Arand, M.; Zou, J.; Archelas, A.; Bottalla, A. L.; Naworyta, A.; Mowbray, S. L., Directed Evolution of an Enantioselective Epoxide Hydrolase: Uncovering the Source of Enantioselectivity at Each Evolutionary Stage. *J Am Chem Soc* **2009,** 131, 7334-43.

7. Reetz, M. T.; Jaeger, K. E., Enantioselective Enzymes for Organic Synthesis Created by Directed Evolution. *Chemistry* **2000,** 6, 407-12.

8. Reetz, M. T.; Wu, S., Laboratory Evolution of Robust and Enantioselective Baeyer-Villiger Monooxygenases for Asymmetric Catalysis. *J Am Chem Soc* **2009,** 131, 15424-32.

9. Turner, N. J., Directed Evolution Drives the Next Generation of Biocatalysts. *Nat Chem Biol* **2009,** 5, 567-73.

10. Ema, T.; Fujii, T.; Ozaki, M.; Korenaga, T.; Sakai, T., Rational Control of Enantioselectivity of Lipase by Site-Directed Mutagenesis Based on the Mechanism. *Chem Commun (Camb)* **2005,** 4650-1.

11. Ema, T.; Kamata, S.; Takeda, M.; Nakano, Y.; Sakai, T., Rational Creation of Mutant Enzyme Showing Remarkable Enhancement of Catalytic Activity and Enantioselectivity toward Poor Substrates. *Chem Commun (Camb)* **2010,** 46, 5440-2.

12. Magnusson, A. O.; Takwa, M.; Hamberg, A.; Hult, K., An *S*-Selective Lipase Was Created by Rational Redesign and the Enantioselectivity Increased with Temperature. *Angew Chem Int Ed Engl* **2005,** 44, 4582-5.

13. Henke, E.; Bornscheuer, U. T.; Schmid, R. D.; Pleiss, J., A Molecular Mechanism of Enantiorecognition of Tertiary Alcohols by Carboxylesterases. *Chembiochem* **2003,** 4, 485-93.

14. Harris, R. H.; Vavra, I., Ketoprofen. In Rainsford, D. K. (Ed.), Anti-Inflammatory and Anti-Rheumatic Drugs: Inflammation Mechanisms and Actions of Traditional Drugs. CRC Press: Boca Raton, **1985**; Vol. 2, p 151-69.

15. Hayball, P. J., Chirality and Nonsteroidal Anti-Inflammatory Drugs. *Drugs* **1996,** 52 Suppl 5, 47-58.

16. Carabaza, A.; Cabre, F.; Rotllan, E.; Gomez, M.; Gutierrez, M.; Garcia, M. L.; Mauleon, D., Stereoselective Inhibition of Inducible Cyclooxygenase by Chiral Nonsteroidal Antiinflammatory Drugs. *J Clin Pharmacol* **1996,** 36, 505-12.

17. Ghezzi, P.; Melillo, G.; Meazza, C.; Sacco, S.; Pellegrini, L.; Asti, C.; Porzio, S.; Marullo, A.; Sabbatini, V.; Caselli, G.; Bertini, R., Differential Contribution of R and S Isomers in Ketoprofen Anti-Inflammatory Activity: Role of Cytokine Modulation. *J Pharmacol Exp Ther* **1998,** 287, 969-74.

18. Ossipov, M. H.; Jerussi, T. P.; Ren, K.; Sun, H.; Porreca, F., Differential Effects of Spinal (*R*)-Ketoprofen and (*S*)-Ketoprofen against Signs of Neuropathic Pain and Tonic

Nociception: Evidence for a Novel Mechanism of Action of (R)-Ketoprofen against Tactile Allodynia. *Pain* **2000,** 87, 193-9.

19. Thayer, A. M., Chemical and Engineering News. Biocatalyst: Houston, 2001.

20. U. S. Food and Drug Administration, FDA's Policy Statement for the Development of New Stereoisomeric Drugs. Chirality, **1992**; 4, 338-40.

21. Tomaszewski, J.; Rumore, M. M., Stereoisomeric Drugs: FDA's Policy Statement and the Impact on Drug Development. *Drug Development and Industrial Pharmacy* **1994,** 20, 119-39.

22. Ong, A. L.; Kamaruddin, A. H.; Bhatia, S., Current Technologies for the Production of (S)-Ketoprofen: Process Perspective. *Process Biochemistry* **2005,** 40, 3526-35.

23. Yoon, S.; Kim, S.; Ryu, Y.; Kim, T. D., Identification and Characterization of a Novel (*S*)-Ketoprofen-Specific Esterase. *Int J Biol Macromol* **2007,** 41, 1-7.

24. Kim, S.; Joo, S.; Yoon, S.; Kim, S.; Moon, J.; Ryu, Y.; Kim, K. K.; Kim, T. D., Purification, Crystallization and Preliminary Crystallographic Analysis of Est-Y29: A Novel Oligomeric Beta-Lactamase. *Acta Crystallogr Sect F Struct Biol Cryst Commun* **2009,** 65, 310-2.

25. Ngo, T. D.; Ryu, B. H.; Ju, H.; Jang, E. J.; Kim, K. K.; Kim, T. D., Crystallographic Analysis and Biochemical Applications of a Novel Penicillin-Binding Protein/Beta-Lactamase Homologue from a Metagenomic Library. *Acta Crystallogr D Biol Crystallogr* **2014,** 70, 2455-66.

26. Jin, J. N.; Lee, S. H.; Lee, S. B., Enzymatic Production of Enantiopure Ketoprofen in a Solvent-Free Two-Phase System. *Journal of Molecular Catalysis B: Enzymatic* **2003,** 26, 209-16.

27. Otwinowski, Z.; Minor, W., Processing of X-Ray Diffraction Data Collected in Oscillation Mode. *Macromolecular Crystallography, Pt A* **1997,** 276, 307-26.

28. Vagin, A.; Teplyakov, A., Molecular Replacement with Molrep. *Acta Crystallogr D* **2010,** 66, 22-5.

29. Winn, M. D.; Murshudov, G. N.; Papiz, M. Z., Macromolecular Tls Refinement in Refmac at Moderate Resolutions. *Methods Enzymol* **2003,** 374, 300-21.

30. Steiner, R. A.; Lebedev, A. A.; Murshudov, G. N., Fisher's Information in Maximum-Likelihood Macromolecular Crystallographic Refinement. *Acta Crystallogr D Biol Crystallogr* **2003,** 59, 2114-24.

31. Adams, P. D.; Afonine, P. V.; Bunkoczi, G.; Chen, V. B.; Davis, I. W.; Echols, N.; Headd, J. J.; Hung, L. W.; Kapral, G. J.; Grosse-Kunstleve, R. W.; McCoy, A. J.; Moriarty, N. W.; Oeffner, R.; Read, R. J.; Richardson, D. C.; Richardson, J. S.; Terwilliger, T. C.; Zwart, P. H., Phenix: A Comprehensive Python-Based System for Macromolecular Structure Solution. *Acta Crystallogr D* **2010,** 66, 213-21.

32. Laskowski, R. A.; MacArthur, M. W.; Moss, D. S.; Thornton, J. M., Procheck: A Program to Check the Stereochemical Quality of Protein Structures. *Journal of Applied Crystallography* **1993,** 26, 283-91.

33. Tian, W.; Chen, C.; Lei, X.; Zhao, J.; Liang, J., Castp 3.0: Computed Atlas of Surface Topography of Proteins. *Nucleic Acids Res* **2018,** 46, W363-W7.

34. Heo, L.; Park, H.; Seok, C., Galaxyrefine: Protein Structure Refinement Driven by Side-Chain Repacking. *Nucleic Acids Res* **2013,** 41, W384-8.

35. Sanner, M. F., Python: A Programming Language for Software Integration and Development. *J Mol Graph Model* **1999,** 17, 57-61.

36. Trott, O.; Olson, A. J., Software News and Update Autodock Vina: Improving the Speed and Accuracy of Docking with a New Scoring Function, Efficient Optimization, and Multithreading. *J Comput Chem* **2010,** 31, 455-61.

37. Fuhrmann, J.; Rurainski, A.; Lenhof, H. P.; Neumann, D., A New Lamarckian Genetic Algorithm for Flexible Ligand-Receptor Docking. *J Comput Chem* **2010,** 31, 1911-8.

38. Lee, G. R.; Heo, L.; Seok, C., Effective Protein Model Structure Refinement by Loop Modeling and Overall Relaxation. *Proteins* **2016,** 84 Suppl 1, 293-301.

39. Baek, M.; Shin, W. H.; Chung, H. W.; Seok, C., Galaxydock Bp2 Score: A Hybrid Scoring Function for Accurate Protein-Ligand Docking. *J Comput Aided Mol Des* **2017,** 31, 653-66.

40. Lee, G. R.; Seok, C., Galaxy7tm: Flexible Gpcr-Ligand Docking by Structure Refinement. *Nucleic Acids Res* **2016,** 44, W502-6.

41. Hudson, K. L.; Bartlett, G. J.; Diehl, R. C.; Agirre, J.; Gallagher, T.; Kiessling, L. L.; Woolfson, D. N., Carbohydrate-Aromatic Interactions in Proteins. *J Am Chem Soc* **2015,** 137, 15152-60.

42. Sheldon, R. A.; Pereira, P. C., Biocatalysis Engineering: The Big Picture. *Chem Soc Rev* **2017,** 46, 2678-91.

43. Duan, G.; Chen, J. Y., Racemic Temperature and Stereochemistry. *Trends in Biotechnology* **1997,** 15, 333.

44. Jin, X.; Liu, B.; Ni, Z.; Wu, Q.; Lin, X., A Novel Control of Enzymatic Enantioselectivity through the Racemic Temperature Influenced by Reaction Media. *Enzyme Microb Technol* **2011,** 48, 454-7.

45. Liu, J.; Zhang, Y.; Qiu, L.; Yang, F.; Ye, L.; Xia, Y., Kinetic Resolution of Ketoprofen Ester Catalyzed by Lipase from a Mutant of Cbs 5791. *J Ind Microbiol Biotechnol* **2004,** 31, 495-9.

46. Kim, J.; Kim, S.; Yoon, S.; Hong, E.; Ryu, Y., Improved Enantioselectivity of Thermostable Esterase from Archaeoglobus Fulgidus toward (*S*)-Ketoprofen Ethyl Ester by

Directed Evolution and Characterization of Mutant Esterases. *Appl Microbiol Biotechnol* **2015,** 99, 6293-301.

TOC

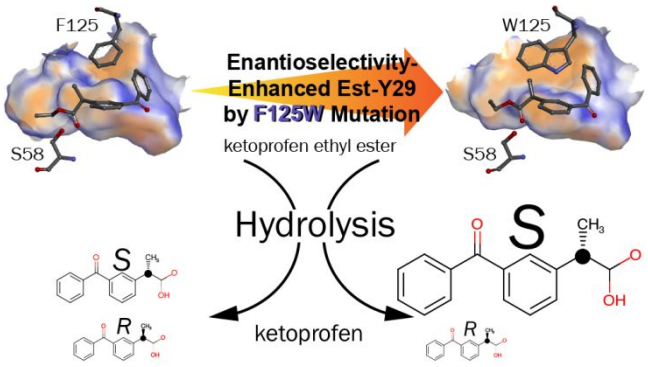
F125
S58
Enantioselectivity-
Enhanced Est-Y29
by F125W Mutation
ketoprofen ethyl ester
W125
S58
Hydrolysis
S
R
ketoprofen
S
R
CH3
O
OH